Millimeter-Wave Base Station Diversity for 5G Coordinated Multipoint (CoMP) Applications

George R. MacCartney, Jr., *Student Member, IEEE* and Theodore S. Rappaport, *Fellow, IEEE*
NYU WIRELESS
NYU Tandon School of Engineering, New York University

Abstract—Millimeter-wave (mmWave) will be used for fifth-generation (5G) wireless systems. While many recent empirical studies have presented propagation characteristics at mmWave bands, macrodiversity and Coordinated Multipoint (CoMP) have not been carefully studied. This paper describes a large-scale mmWave base station diversity measurement campaign at 73 GHz in an urban microcell (UMi) in downtown, Brooklyn, New York, and provides the first detailed analysis of CoMP and macrodiversity performance based on extensive measurements. The research employed nine different base station locations in a 200 m by 200 m area and considered 36 individual transmitter-receiver combinations for extensive co- and cross-polarized varying directional beam channel impulse response measurements. From the measured data, hypothesis testing with cross-validation shows that large-scale shadow fading of directional path loss at an RX from multiple base stations can be modeled as being independent. To consider life-like human blockage in CoMP and macrodiversity analysis, simulated human blockage traces are superimposed on the directional measurements to quantitatively show that a user that is served by multiple base stations undergoes dramatically less outage in the presence of rapid fading events, compared to a single serving base station. Moreover, the base station diversity measurements are used to determine the effectiveness of downlink precoding techniques for mmWave CoMP. While results show that coordination can improve network performance by suppressing interference when it exists, nearly half of the 680,000 directional CoMP measurements ($\sim 43\%$) result in no interference for either user, meaning that macrodiversity alone may offer sufficient link and capacity improvement and that CoMP may not be necessary for interference coordination at mmWave when narrow directional beams are used.

Index Terms—Millimeter-wave, 73 GHz, path loss, channel model, CoMP, 5G, diversity, macrodiversity, beamforming, coordinated multipoint.

I. INTRODUCTION

Enhanced mobile broadband (eMBB) with 10-Gb/s peak throughput rates will be available in the coming years as 5G wireless networks are deployed [1]. The limited availability of crowded sub-6 GHz spectrum and the vast amount of unused spectrum at millimeter-wave (mmWave) frequencies provides motivation for the investigation of mmWave bands for 5G wireless systems [2]. To meet the impending spectrum crunch,

researchers explored the viability of mmWave bands for 5G cellular [2]–[5]. While a majority of experimental measurements at mmWave have focused on propagation characteristics, little work has been done or made available on base station (BS) diversity in an urban microcell (UMi). This paper is the first in-depth study of macrodiversity and CoMP, based on extensive directional measurements made with nine BS locations on the NYU Brooklyn engineering campus.

A. Base Station Diversity

Base station (BS) diversity or macrodiversity has been shown to combat outage in traditional cellular networks. Macrodiversity exploits either independent or highly uncorrelated propagation paths between multiple BSs and a mobile [6], [7]. BS diversity studies at mmWave frequencies have mainly focused on fixed wireless. Cell-site diversity was studied as a method to mitigate the effects of rain and vegetation attenuation in [8], [9]. In early LMDS studies, polarization interleaving between neighboring BSs was shown to increase signal-to-interference (SIR) by several dB, although, depolarization from foliage and rain resulted in limited improvement or even degradation due to co-channel interference [10]. LMDS simulations in [11] revealed that using highly directional antennas at the BS and mobile could dramatically improve system performance by reducing co-channel interference, and system outage by an order of magnitude [11].

While earlier studies on LMDS diversity focused on polarization diversity, Le *et al.* studied BS diversity for links of less than 1 km in order to overcome adverse effects from rain at centimeter-wave (cmWave) and mmWave bands [12]. Measurements were conducted at 25 GHz over 20 MHz of bandwidth and at 38 GHz over 200 MHz of bandwidth using 29 dBi and 32 dBi high-gain antennas at 25 GHz and 38 GHz, respectively. Results in [12] showed that as the spatial separation between BSs increased, site diversity gain increased. Diversity gain was also shown to increase as angle separation between the mobile and two BSs increased, a conclusion also made for lower UHF bands.

B. Coordinated Multipoint (CoMP)

Coordinated multipoint (CoMP) is commonly used for diversity and interference suppression, and was first introduced by Foschini and Karakayali [13]. CoMP relies on multiple BSs or transmission points (TP), and network coordination between

TPs to increase network efficiency and throughput, and is often referred to as network *multiple-input and multiple-output (MIMO)*. CoMP is primarily used to mitigate interference at the UE, where channel state information (CSI) experienced at the UE is shared between BSs in order to coordinate simultaneous or scheduled downlink transmissions while jointly processing mobile uplink signals. A high-speed backbone network is necessary for transfer of CSI between BSs for reliable coordination [14]. Due to large potential theoretical gains, CoMP [13] was introduced as a study item for LTE systems in 3GPP TR 36.814 Release 9 and was added as a new feature for LTE-Advanced (LTE-A) in 3GPP TR 36.819 Release 11 [15]. Using 3GPP CoMP nomenclature, a "point" is a set of co-located transmit antennas (same geographical site), but where sectors of the same site correspond to different points [15], [16]. The 3GPP Release 11 defined downlink CoMP categories for joint processing (JP) which include joint transmission (JT) and dynamic point selections (DPS), or coordinated scheduling/coordinated beaming (CS/CB), all of which require CSI [15], [16]. Applying similar concepts for mmWave networks is a growing interest and motivation for the work in this paper.

C. MmWave and CoMP Experiments

To date, there have been limited experiments for downlink BS diversity and CoMP at mmWave. NTT Docomo and Ericsson conducted experiments at 15 GHz with a 5G radio access prototype with two TPs and one mobile [17]. Downlink CoMP was shown to improve throughput by 70% and 30% in small (20 m × 20 m) and large (100 m × 70 m) coverage areas, respectively, exceeding 10 Gbps speeds when the two TPs were separated by more than 50 m. A follow-up study in [18] investigated CoMP with two TPs and showed that spatial multiplexing in LOS improved performance from 5.7 bps/Hz to 12.6 bps/Hz. For large angular separation between the two TPs and the UE (approaching 180°), rank-4 transmission was consistent with a maximum achievable spectral efficiency of 13 bps/Hz [18]. Additional measurements by Kurita *et al.* in [19] showed that spatial multiplexing gains and throughput significantly improved as the spacing between TPs increased, where overall performance exceeded 10 Gbps with TPs separated by 50 m. Work in [16] also shows rank-4 is possible, but rare. Other than [17], [18], [20], little work exists on BS diversity and CoMP at mmWave bands at least in terms of real-world measurements.

D. Contributions of This Work

Due to lack of measurement-based studies on mmWave BS diversity, we utilize mmWave measurements from a large-scale BS diversity measurement campaign to investigate the effects of BS diversity and CoMP networks such as fading at the user, user coverage and outage, and network performance improvement. By incorporating real-world 73 GHz mmWave propagation data we provide some of the first extensive analysis on the effects of BS diversity and CoMP at mmWave in a UMi. The main contributions of this paper are as follows:

- To better understand real-world BS diversity and CoMP at mmWave, we conducted a large-scale measurement campaign using directional high-gain and narrowbeam antennas using 1 GHz wide RF signals at the 73 GHz carrier frequency and measured tens of thousands of channel impulse responses (CIRs) [20], as described in Section II.
- In Section III we provide directional and omnidirectional CI path loss models derived from the measurement campaign using nine BSs and a total of 36 TX-RX radio links.
- The BS diversity measurements are utilized in Section IV to provide analysis on the correlation of shadow fading from multiple BSs to a receiver. The correlation of shadow fading at mmWave is important to understand when simulating channels and estimating diversity gains at mmWaves. We show through hypothesis testing and cross-validation that it is reasonable to consider shadow fading independent among multiple BSs to an RX.
- The effects of BS diversity in the presence of human blockers is crucial to understand for future mmWave networks since humans have been shown to cause rapid fading and signal degradation due to narrow beams at mmWave [21]. Thus, in Section V we analyze such effects on outage by combining BS diversity measurements with simulated human blockage events.
- Because it was shown that CoMP could significantly improve spectral efficiency of networks at LTE bands, and since there was growing interest for the same at mmWave bands but a lack of real-world measurements on the topic, we set out to study the impact of CoMP at mmWave. In Section VI we aggregate the BS diversity measurements to analyze the effectiveness of CoMP and downlink precoding techniques for interference mitigation at mmWave in a UMi environment and discuss the practicality of considering such techniques. Conclusions of our studies are given in Section VII.

II. MEASUREMENT CAMPAIGN AND HARDWARE

A. Measurement Environment and Locations

The mmWave BS diversity measurements were conducted in the summer of 2016 on the NYU engineering campus in order to gain knowledge for mmWave networks that exploit macrodiversity and CoMP [16], [20], [22]. Portable BSs were deployed at a height of 4 m above ground level (AGL), with a range of 3 to 5 different receiver (RX) locations for each BS. The NYU engineering campus is built around an orchard of cherry trees that is surrounded by an open square (O.S.) in downtown Brooklyn, New York and as shown in Fig. 1, spanned a ∼200 m by 200 m area, representing a typical urban UMi scenario. The courtyard is surrounded by buildings of up to fifteen stories on all sides, with urban canyon streets at each corner.

The measurement locations used a wide range of TX and RX locations, distances, and environments (LOS and NLOS). To emulate a small-cell deployment, 11 locations (yellow stars in Fig. 1) were selected as TX BSs and were in areas
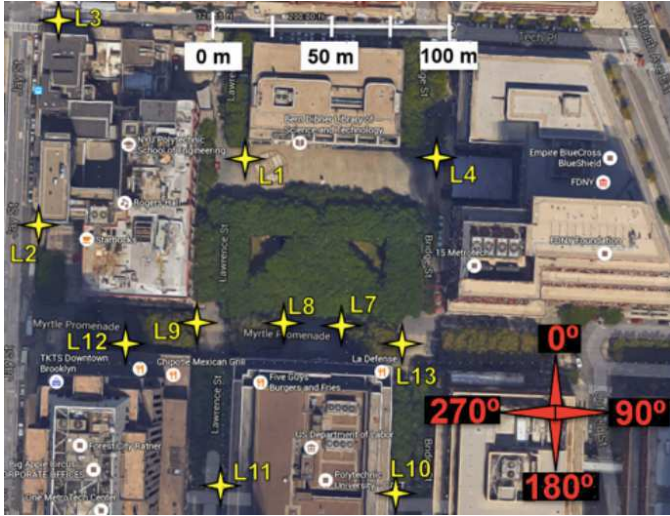
Fig. 1: TX and RX locations for BS diversity measurements at NYU.

TABLE I: List of TX locations used to transmit to each RX and range of T-R separation distances. A map of locations is provided in Fig. 1.

RX Location	Serving TX Location	T-R Dist. Range (m)
L1	L3,L4,L7,L11,L13	$80 \leq d \leq 140$
L2	L3,L9,L12	$61 \leq d \leq 78$
L3	L2	77
L4	L1,L3,L7,L10,L13	$80 \leq d \leq 170$
L7	L1,L2,L4,L10	$72 \leq d \leq 133$
L8	L1,L7,L9	$21 \leq d \leq 78$
L9	L1,L2,L4,L11	$63 \leq d \leq 123$
L10	L4,L7,L13	$59 \leq d \leq 140$
L12	L1,L2,L4,L7,L11	$61 \leq d \leq 149$
L13	L1,L4,L10	$59 \leq d \leq 107$

representative of high user concentrations, and which also served as RX locations at 1.4 m heights to emulate web-browsing at the RX. Of the 11 locations in Fig. 1, on any given measurement day, one of them was chosen as the TX location, and some of the others were used as RX locations, for measuring CIRs. The experiment considered up to three diversity BSs to measure a diverse range of distances, angular separations, and environments. 36 total TX-RX radio links were tested using 11 LOS and 25 NLOS TX-RX links, where signals were received from three or more TX locations at nine RX locations, and where eight TX locations were used to transmit to three or more RX locations. Received power, outage, and best beam angles across various antenna pointing angles for each RX and multiple TXs were recorded. 3D transmitter-receiver (T-R) separation distances ranged from 21 m to 140 m in LOS, and 59 m to 170 m in NLOS. Table I indicates the locations used for TX-RX combinations, their corresponding T-R separation distance ranges, and common TXs for a given RX.

B. Measurement Hardware, Specifications, and Procedures

The BS diversity measurement campaign was conducted using an absolute-timing ultra-wideband sliding correlator channel sounder from [23], transmitting with 1 GHz of RF null-to-null bandwidth at a center frequency of 73.5 GHz [20], [23]. The system used rotatable directional horn antennas with a 7° azimuth/elevation (Az./El.) half-power beamwidth

(HPBW) and 27 dBi of gain at the TX, and 15° Az./El. HPBW with 20 dBi of gain at the RX. The max output power was 14.9 dBm into the TX antenna and the maximum EIRP was 41.9 dBm, with a max measurable path loss of 175 dB. Narrowbeam directional antennas at the TX and RX emulate future mmWave systems that will consist of adaptable directional beams from a BS, with somewhat broader beamwidths steerable at a mobile. The TX antennas were scanned over 120° sectors and RX antennas were rotated across the entire 360° azimuth plane at three separate elevations for each particular TX pointing angle [20], [23]. The TX antenna for each TX-RX link combination was rotated in 8° increments to span a 120° sector (15 pointing angles), representative of a typical panel BS, with the strongest TX angle at the center of the sector. For each of the 15 TX pointing angles, the RX antenna with 15° HPBW was scanned in 15° increments across the entire 360° azimuth, at the fixed elevation angle that resulted in the strongest received power, resulting in 24 discrete angle measurements per azimuth scan. A power delay profile (PDP) channel impulse response with 2 ns multipath component (MPC) time resolution was recorded for each unique TX-RX angle combination for where a signal was detectable. The RX antenna azimuth scanning was then repeated for two additional elevation angles, which were ±15° on either side of the strongest elevation angle. Each TX-RX link combination resulted in 45 azimuth angle measurement scans for co-polarized vertical-to-vertical (V-V) antennas. The same procedure was repeated for cross-polarized vertical-to-horizontal (V-H) antennas, resulting in 90 azimuth angle scans for a single TX-RX combination. A maximum of 2,160 PDPs were recorded for each TX-RX combination, but 700 PDPs on average were used for analysis for each combination since angles where a signal was not detectable were not recorded and PDPs with SNR of 5 dB or less were discarded via thresholding in post-processing [20], [23].

C. Measurement Outputs

More than 130 GBs of data were recorded, from 38,880 and 27,567 V-V and V-H PDPs, respectively. Post-processing to remove PDPs that did not meet a 5 dB SNR noise floor requirement resulted in 18,183 V-V PDPs for analysis (V-H PDPs were not processed for this paper). From the single TX-RX location combinations we found: 54 combinations of 2 common TXs to 1 RX, 42 combinations of 3 common TXs to 1 RX, and 34 combinations of 2 common TXs to 2 common RXs. Using the best 100 beams (strongest received power) for each individual TX-RX combination, the following diversity and CoMP related network realizations (beam combinations) are used for analysis in Sections V and VI: $36 \times 100 = 3,600$ measurement/network realizations for 1 TX to 1 RX, $54 \times 100^2 = 540,000$ measurement/network realizations for 2 TXs to 1 RX, and $42 \times 100^3 = 42,000,000$ measurement/network realizations for 3 TXs to 1 RX. The data also provided $2 \times 34 \times 100^2 = 680,000$ network settings/realizations for 2 common TXs and 2 common RXs when each TX transmits a single beam to a paired RX, such that each RX has a beam with energy from the TX transmitting to it, but may experience interference from the TX transmitting to the other RX.

TABLE II: Directional path loss model terminology.

| Setting	Description
LOS-B	TX and RX locations have a clear optical path and antenna are perfectly-aligned on boresight.
LOS-NB	TX and RX locations have a clear optical path but the antennas are not boresight-aligned.
NLOS	No clear optical path between the TX and RX antennas (covers all TX and RX arbitrary pointing angles).
NLOS-Best	NLOS unique antenna pointing angle combinations with strongest received power for each NLOS TX-RX location pair.
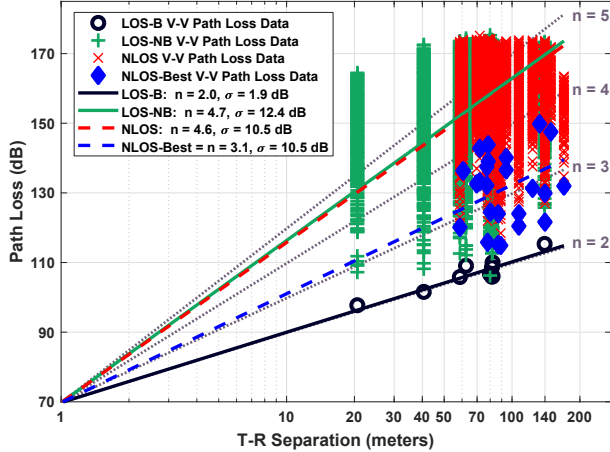
Fig. 2: Directional CI V-V UMi path loss models for unique pointing angles between the TX and RX where signal could be received [20].

III. PROPAGATION RESULTS AND ANALYSIS

UMi O.S. path loss models were determined from the BS diversity directional measurements [20], [22]. We use close-in free space reference distance (CI) path loss model that is written in 3GPP-style format as [3], [24]:

$$\mathrm{PL}^{\mathrm{CI}}(f_c, d)[\mathrm{dB}] = 32.4 + 10n\log_{10}(d) + 20\log_{10}(f_c) + \chi_\sigma \quad (1)$$

where d is the 3D Euclidean distance between the TX and RX, f_c is the carrier frequency in GHz, n is the PLE with antenna gains removed [3], [25], and 32.4 is FSPL in dB at 1 GHz at 1 m. The zero-mean Gaussian random variable χ_σ with standard deviation σ (in dB) represents shadow fading. The use of 1 m as a reference distance allows path loss to be tied to a true physical anchor point [3]. The CI model in (1) is chosen since the model parameters have been shown to be more stable and accurate across frequencies and distances [24]. Directional wideband received power ($P_{r(\mathrm{dir.})}$) from measurable PDPs at specific TX/RX pointing angles was calculated by integrating the area under each PDP with both a -20 dB max peak and +5 dB noise floor SNR threshold [23], where path loss for each directional TX/RX antenna pointing angle pair was calculated while removing the TX and RX antenna gains in the PDP processing [26]. Environment descriptions for directional path loss are slightly different than previously used in the literature [3], [22], to better represent propagation characteristics for mmWave directional path loss models. The mmWave regime requires directional and high-gain antennas to measure path loss at large distances, meaning that measurements come from narrow directional paths for

TABLE III: 73 GHz directional CI V-V path loss model (1) parameters for the UMi O.S., with TX heights of 4 m and RX heights of 1.4 m [20], [22].

73 GHz VV Directional CI Path Loss Models for $d_0 = 1$ m			
LOS-B		LOS-NB	
PLE	σ [dB]	PLE	σ [dB]
2.0	1.9	4.7	12.4
NLOS		NLOS-Best	
PLE	σ [dB]	PLE	σ [dB]
4.6	10.5	3.1	10.5

TABLE IV: 73 GHz omnidirectional CI V-V path loss model (1) parameters for TX heights of 4 m and RX heights of 1.4 m.

73 GHz Omnidirectional CI Path Loss Models for $d_0 = 1$ m			
LOS		NLOS	
PLE	σ [dB]	PLE	σ [dB]
1.9	1.7	2.8	8.7

specific AODs and AOAs. Therefore, new descriptions for directional path loss models are defined in Table II.

Fig. 2 shows the measured directional path loss data and CI path loss model (1) for directional measurements and V-V antennas. In Fig. 2, the LOS-Boresight (LOS-B) CI path loss model has a PLE of $n = 2.0$ which perfectly matches Friis' free space transmission formula [27]. The small standard deviation of 1.9 dB indicates little macrodiversity differences on boresight-to-boresight links. The LOS-non-boresight (LOS-NB) directional PLE of $n = 4.7$ reveals high attenuation as a function of distance for antennas that are not boresight aligned in LOS. There are some secondary LOS-NB angles that are within 5 to 10 dB power of the main LOS-B angles which could be used to maintain a link in the event of a blockage or outage of the main LOS path. Furthermore, the LOS-NB shadow fading standard deviation of 12.4 dB indicates off-boresight angles in a LOS mmWave UMi scenario can drastically vary around the distant-dependent mean value in a BS macrodiversity system. The NLOS CI PLE of $n = 4.6$ is nearly identical to the PLE of 4.7 from earlier 73 GHz measurements in a typical UMi in Manhattan at 73 GHz [3]. A surprising result was the PLE of $n = 3.1$ for the NLOS-Best pointing angles in NLOS. The NLOS-Best PLE shows that if the TX and RX antennas optimally point their beams, path loss can be greatly reduced in NLOS compared to arbitrary pointing angles [3]. The large improvement in link margin for the best TX-RX pointing angle combinations are likely caused by tall buildings around the courtyard that reflect energy to create a multipath rich propagation scenario. The NLOS and NLOS-Best shadow fading standard deviations of 10.5 dB each, are comparable to [3]. The CI path loss model parameters for the V-V directional measurements are provided in Table III. Omnidirectional pass loss models from the measured data are given in Table IV (refer to [20], [22] for more details).

IV. SHADOW FADING CORRELATION FOR MACRODIVERSITY

Macrodiversity has been used to combat large-scale shadow fading by use of geographically separated BSs [28], [29]. If two or more BSs are separated geographically by some unknown distance and also by angle to a mobile, then it is likely that the signal propagation paths to the mobile are uncorrelated, hence, shadow fading is uncorrelated. Since

shadow fading is commonly modeled by a Gaussian random variable, uncorrelated Gaussian shadow fading implies independent shadow fading [7], [26]. It is more favorable if the signal propagation paths are independent, rather than just uncorrelated, since it would allow for random drops in simulations, without the need for joint distributions of diversity signals, since jointly Gaussian random variables are independent if they are uncorrelated [7]. Macrodiversity has been extensively studied for UHF and microwave bands [28], [29], but experimental measurements for mmWave macrodiversity in UMi scenarios have not been available until this work. In this Section we formulate a problem for studying shadow fading correlation with the BS diversity measurements, outline steps for hypothesis testing with cross-validation, and discuss results.

A. Hypothesis Testing for Independent Macrodiversity

Typically, downlink measurements to an RX arrive from BSs that transmit with sectored antennas where a mobile measures path loss along a route [29]. Shadow fading values from multiple BSs are then used to determine a covariance matrix of shadow fading among multiple BSs and a mobile [30], which can provide insight into how correlated shadow fading is among the BSs and a mobile. Our goal is to determine whether the signals received at a user from geographically separated BSs are more likely to experience independent large-scale shadow fading when directional antennas are used (assuming individual links at mmWave experience Gaussian shadow fading [3]), or if it is more likely that shadow fading is correlated among multiple BSs transmitting to a single RX. We test whether or not shadow fading from two or more BSs is correlated or not through hypothesis testing, for the null hypothesis H_0, associated with independent fading (e.g. uncorrelated Gaussian), and the alternative hypothesis, H_1, representing correlated shadow fading. The BS diversity measurements were designed to encompass diverse environments and various T-R separation distances using extensive narrow-beam and directional antenna measurements at the TX and RX. For hypothesis testing, nine RX locations were selected that had three or more TX locations (see Table I and map in Fig. 1). For each RX i with $i \in \{1, 2, 4, 7, 8, 9, 10, 12, 13\}$, the three closest TX locations to the RX are identified and the shadow fading values from each TX to RX i are represented by a vector $\mathbf{x}_i = [x_{i1}, x_{i2}, x_{i3}]^T$, where x_{ij} denotes the shadow fading (in dB) from the jth closest TX to RX i. The shadow fading values are calculated by using the directional CI path loss models from Table III at the specific T-R separation distances from the measurements using (1), according to the designated environment (LOS or NLOS), for each individual TX-RX location combination. The steps in the following section outline how the shadow fading values are used for the hypothesis testing for shadow fading from multiple BSs. Although only nine RX locations were used, there were 54 sets of two TX to one RX and 42 sets of three TX to one RX combinations which are used here for hypothesis testing analysis.

B. Steps for Shadow Fading Uncorrelated Hypothesis Testing

The calculated shadow fading vectors $\mathbf{x}_i$ are assumed to be realizations of a zero-mean multivariate Gaussian distribution, $\mathbf{x}_i \sim \mathcal{N}(\mathbf{0}, \mathbf{Q})$, with probability density:

$$p_\mathbf{x}(\mathbf{x}_i | \mathbf{Q}) = \frac{1}{(2\pi)^{d/2} |\mathbf{Q}|^{1/2}} \exp\left(-\frac{1}{2}\mathbf{x}_i^T \mathbf{Q}^{-1} \mathbf{x}_i\right) \quad (2)$$

where d is the number of parameters / dimensions and in our case is three for the closest three BSs to the RX, and $\mathbf{Q}$ is a 3×3 covariance matrix. The shadow fading data is organized as an $N \times d$ matrix or 9×3 for $N = 9$ realizations (9 RX locations) and $d = 3$ parameters (3 BSs), $\mathbf{X} = [\mathbf{x}_1, \mathbf{x}_2, \mathbf{x}_4, \mathbf{x}_7, \mathbf{x}_8, \mathbf{x}_9, \mathbf{x}_{10}, \mathbf{x}_{12}, \mathbf{x}_{13}]^T$, and due to the limited data set, hypothesis testing is performed with cross-validation. Cross-validation is a typical statistical method used to validate a model by splitting data into training and test sets in order to evaluate how well the model generalizes [31]. Two simple models are suggested for cross-validation here due to the limited data set, since a more complex model will likely over-fit the data and perform worse than the simpler models [32]. The testing is done for:

- Null hypothesis H_0: independent (uncorrelated) Gaussian shadow fading, $\mathbf{x}_i \sim \mathcal{N}(\mathbf{0}, \mathbf{Q}_0) \ \forall i$, $\mathbf{Q}_0 = a \cdot I_3$, where I_3 is the 3×3 identity matrix.
- Alternative hypothesis H_1: correlated shadow fading, $\mathbf{x}_i \sim \mathcal{N}(\mathbf{0}, \mathbf{Q}_1) \ \forall i$,
  $$\mathbf{Q}_1 = \begin{bmatrix} a & b & b; b & a & b; b & b & a \end{bmatrix}.$$

With hypotheses H_0 and H_1, log-likelihoods and cross-validation [33] are used to determine which is more likely. The log-likelihood function of the zero-mean multivariate Gaussian distribution in (2) is re-written to maximize the likelihood and is simplified by ignoring constants and independent terms as shown here:

$$-\log(p_\mathbf{x}(\mathbf{x}_i | \mathbf{Q})) = \frac{1}{2}\log|\mathbf{Q}| + \frac{1}{2}\mathbf{x}_i^T \mathbf{Q}^{-1} \mathbf{x}_i \quad (3)$$

Cross-validation testing is performed via the leave-one-out method [32] by first removing one of the $N = 9$ realizations $\mathbf{x}_i$ from matrix $\mathbf{X}$, which is used as the test set, and the remaining $N-1 = 8$ realizations are used as the training set $\tilde{\mathbf{X}} = [\tilde{x}_{m,k}]$, which is an 8×3 matrix, and this procedure is repeated $N = 9$ times. The training set matrix $\tilde{\mathbf{X}}$ is used for determining $\mathbf{Q}$ and $\mathbf{Q}^{-1}$ in (3) for which the test set is applied to when determining the log-likelihoods, where $\mathbf{Q}$ is of the form $\mathbf{Q}_0$ and $\mathbf{Q}_1$, for H_0 and H_1, respectively.

The value of a in $\mathbf{Q}_0$ is determined so as to minimize the log-likelihood function and is calculated as follows:

$$a = \frac{1}{(N-1)d} \sum_{m}^{N-1} \sum_{k}^{N-1} \tilde{x}_{m,k}^2 \quad (4)$$

with $m \in \{1, ..., 8\}$ and $k \in \{1, 2, 3\}$. Calculating a in this way is the same as taking the average of the measured variances from each of the three independent parameters (three BSs). The value of a in $\mathbf{Q}_1$ is similarly calculated with (4), which refers to the mean variances over all parameters (BSs). Since shadow fading is assumed to be correlated for H_1, b in $\mathbf{Q}_1$ is:

$$b = \frac{1}{(N-1)d(d-1)} \sum_{m=1}^{N-1} \sum_{k=1}^{d} \sum_{t \neq k}^{d} \tilde{x}_{m,k}\tilde{x}_{m,t} \quad (5)$$

which represents the average covariance of all shadow fading values. The $\mathbf{Q}_0$ and $\mathbf{Q}_1$ covariance matrices calculated from each training set are then used in (3) along with the test set $\mathbf{x}_i$ that was left out, in order to calculate the log-likelihood value of H_0 and H_1 for each training set. The average log-likelihood values for hypotheses H_0 and H_1 are then used to make a decision on which hypothesis is more likely, where a lower value indicates the hypothesis is more likely [32].

C. Directional Shadow Fading Correlation Results

The shadow fading hypothesis testing was performed for four directional scenarios where the LOS-B and NLOS-Best path loss data were used to calculate shadow fading values for each individual TX-RX location combination by using the path loss models from Table III. The four scenarios are: 1) 9 RX locations and the 2 nearest neighbor BSs serving each of them; 2) all 54 combinations of 2 BSs that transmitted to a common RX; 3) 9 RX locations and the 3 nearest neighbor BSs transmitting to them; 4) all 42 combinations of 3 BSs that transmitted to a common RX. The average log-likelihoods calculated for the H_0 and H_1 hypotheses are provided in Table V. The hypothesis with the lower average log-likelihood is considered to be the more likely hypothesis. For scenarios 1 and 2 we assume an RX receives directional signals simultaneously from 2 BSs, and the average LLs of H_0 and H_1 for each hypothesis test were extremely close and within the standard error of each other. Similar average LL test scores shows that there is no clear differentiation between correlated or independent shadow fading at an RX being transmitted to from two separate BSs. It is common practice to choose a simpler model when LLs are within the standard error (SE) of one another [34]. Thus, we can assume that a more complicated shadow fading model (correlated) is not necessary to use when modeling shadow fading between 2 BSs and an RX at mmWave. Scenario 3 results in a much lower test score for H_0 at 7.95 compared to 8.63 for H_1, indicating that independent (uncorrelated) Gaussian shadow fading is more likely at an RX, compared to correlated shadow fading. When considering all 42 combinations of 3 BSs and a RX, the H_0 test score is higher than H_1, but is within the standard error of H_1, indicating that the null hypothesis can be chosen.

The results here show that it is not necessary to use a more complicated covariance matrix for directional shadow fading between an RX and its closest (in distance) serving BSs. Since the H_0 covariance matrix $\mathbf{Q}_0$ can be used to model shadow fading for the best directional received powers between an RX and its closest BSs, we can make the conjecture that shadow fading is independent among multiple BSs transmitting to an RX and can be modeled and simulated as such. Results for Omnidirectional shadow fading hypothesis testing can be found in [20].

V. COORDINATED MULTIPOINT FOR LINK RELIABILITY

The received power level at a mobile has been shown to be significantly affected by the presence of human blockers at mmWave bands [21], [35]. Using directional narrowbeam

TABLE V: Directional shadow fading hypothesis testing cross-validation results. $\overline{LL}$ is the average log-likelihood across all the tests and $SE(\overline{LL})$ is the sample standard error of the log-likelihood values for each hypothesis.

73 GHz Directional Shadow Fading Hypothesis Testing		
	$\overline{LL}$	$SE(\overline{LL})$
Scenario 1: 9 RXs each with 2 BSs		
H_0	5.08	0.33
H_1	5.16	0.44
Scenario 2: 54 Combinations of an RX with 2 BSs		
H_0	5.12	0.10
H_1	5.08	0.11
Scenario 3: 9 RXs each with 3 BSs		
H_0	7.95	0.16
H_1	8.63	0.36
Scenario 4: 42 Combinations of an RX with 3 BSs		
H_0	8.00	0.16
H_1	7.83	0.36

antennas at mmWave bands results in narrower angular spreads compared to 4G/LTE BSs and mobile devices [21], [26], [36]. Therefore, it is envisioned that mmWave deployments will use a diverse set of BSs to simultaneously serve a single user or use rapid re-routing, as a means to mitigate rapid signal degradation [37], and such a network deployment directly motivated the experimental design of the measurements in Section II [22]. Simultaneous transmission from multiple BSs to mitigate effects of human blockers may be considered a type of macrodiversity or coordinated joint transmission (JT) method [15], [38], and rapid re-routing [37] or selection diversity may be considered a type of dynamic point selection, both of which are downlink CoMP techniques, and which require sharing CSI between BSs. In this section we combine simulations of rapid fading human blockage events [21] with multipoint path loss measurements [22] to estimate the reduced outage in a typical UMi mmWave scenario, where multiple BSs are connected to a central unit (CU) via high-speed backhaul for scheduling and coordination [39].

A. Analysis Use Cases

The 7° antenna HPBW four-state Markov model transition rates from Table V in [21] were used with the shadowing event CDF parameters from Table IV in [21], in order to simulate human blockage traces. Three use-cases: Case 1) one serving BS; Case 2) two simultaneous serving BSs; and Case 3) three simultaneous serving BSs, were investigated by using the 100 best directional antenna beam measurements described in Section II-C, for each individual TX-RX location combination, and superimposing simulated human blockage event attenuation on top of the measurements.

1) Case 1: One Base Station: In order to represent a statistical sense of the potential beams that could be formed between a TX and RX in a real-world scenario and assuming that the TX and RX could steer their beams, the 100 strongest received powers (lowest path loss) for each of the 36 TX-RX location combinations were used for analysis as realistic *data points* of typical user beams in a CoMP deployment. Note that these 100 beams were formed with 7° and 15° HPBW antennas at the TX and RX, respectively. A simulation was setup as a means to use each measured path loss as a data point with BS TX power $P_{TX} = 30\,\text{dBm}$, TX antenna gain $G_{TX} = 27\,\text{dBi}$, RX antenna gain $G_{RX} = 20\,\text{dBi}$ (same as measurements), measurement bandwidth $BW = 1\,\text{GHz}$, average thermal noise
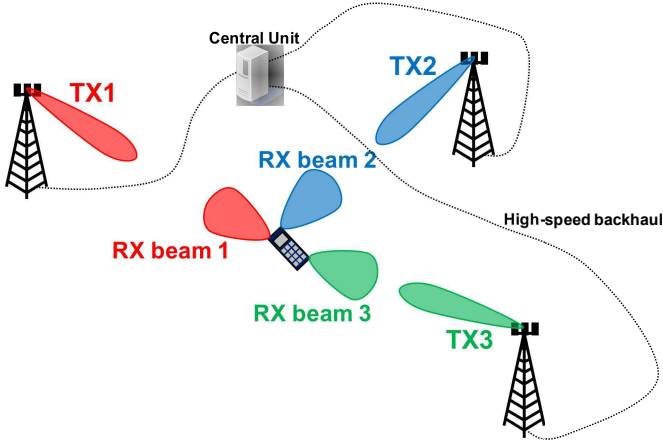
Fig. 3: Sketch of three BSs each forming an RF beam to simultaneously serve a user which can form 3 RF beams for either selecting or combining signals from the BSs. Note that each RX beam is meant for only one TX beam (forced diversity).

TABLE VI: Parameters used to simulate and analyze the effect of simulated rapid fading events with measured path loss values from the measurement campaign.

Parameter	Setting
Total Transmit Power	30 dBm
TX antenna gain	27 dBi
RX antenna gain	20 dBi
Bandwidth	1 GHz
Thermal Noise Power (N_0)	-84 dBm
Noise Figure (NF)	10 dB
Max Measurable Path Loss	175 dB
Path Loss	From measurement campaign – w/o antenna gains (See Fig. 2)
Human Blockage Model	7° HPBW Four-State Markov Model (From [21])

power $N_0 = -84$ dBm, and noise figure $NF = 10$ dB, with parameters also provided in Table VI. In Case 1 (one BS), a BS and user are assumed to have each formed a single RF beam for each of the 36×100 data points, as depicted by the TX 1 and RX 1 beams in Fig. 3. The average received power using real-world path loss (PL_meas) from the measurements and the system parameters identified in Table VI were calculated as shown here:

$$
\begin{aligned}
P_r(d)[\text{dBm}] = &\, P_{TX}[\text{dBm}] + G_{TX}[\text{dBi}] \\
&- PL_\text{meas.}(TX, RX, \theta_{TX}, \theta_{RX}, d)[\text{dB}] + G_{RX}[\text{dBi}]
\end{aligned}
\tag{6}
$$

where $PL_\text{meas.}$ is the measured path loss and is a function of the TX and RX locations, TX antenna pointing angle θ_{TX}, RX antenna pointing angle θ_{RX}, and distance d. SNR in dB was calculated as: $\text{SNR}[\text{dB}] = P_r[\text{dBm}] - (N_0 + NF)$

Next, using the received power calculated from the 36×100 best beams over all TX-RX locations in (6), human blockage simulations are generated and attenuation from the simulations is superimposed on top of the received powers in order to calculate SNR in the presence of random blockage events. The 3GPP TR 38.901 V14.2.0 (Release 14) [40] channel model specifies 5 potential independent blockers per path, therefore, one to five independent rapid fading blockage simulation traces were generated across time for each received power beam. The average mean attenuations for fading events from the four-state Markov model in [21] (and simulated here) were shown to be 15.8 dB. We note here that the fading event

simulations are based on peer-to-peer level measurements [21] and are not representative of transmitters at BS heights to user heights, nevertheless, this was deemed reasonable since at T-R separation distances greater than 40 m or so, BSs are on the horizon and thus are at similar heights, relative to the user. For each random blockage event simulated for each beam, a random and arbitrary time t_i was chosen in order to sum the combined blockage loss in dB across all blockage event traces at time t_i. The individual simulated traces for blockage events are assumed to be ergodic since the average attenuation across time is equal to the average attenuation across multiple traces at a fixed time.

The received power in the event of m blockage events (uniformly distributed between 1 and 5) at an arbitrary time t_i is calculated as:

$$
\begin{aligned}
P_{r_\text{block}}[\text{dBm}] = &\, P_{TX}[\text{dBm}] + G_{TX}[\text{dBi}] - PL_\text{meas.} \\
&+ \sum_{n=1}^{m} L(n, t_i)[\text{dB}] + G_{RX}[\text{dBi}]
\end{aligned}
\tag{7}
$$

where $L(n, t_i)$ is the blockage loss in dB for blockage event n at arbitrary time instant t_i. Thus, the SNR in the presence of blockage events in dB is:

$$
\text{SNR}_\text{block}[\text{dB}] = P_{r_\text{block}}[\text{dBm}] - (N_0 + NF)
\tag{8}
$$

This calculation is made for all 36×100 beam combinations.

2) Case 2: Two Base Stations: The measurement campaign resulted in 54 sets of combinations where 2 common TX locations transmitted to 1 RX location. For Case 2, it was assumed that the RX could simultaneously form 2 separate RF beams by using two transceivers, for either selecting or combining signals from two serving TXs. Fig. 3 displays an example of two TXs (TX1 and TX2) and an RX with two RF beams (beam 1 and beam 2), one for each TX. We note that each RX beam can be used for only one TX, such that we are forcing BS diversity in this analysis. In order to consider a number of strong beams between each TX and RX, the 100 strongest received power beams between each TX and the RX were used as received power data points, resulting in 54×100^2 user beam combinations (*data points*) for 2 TXs to one RX. For each of the measured user beams, the same blockage model in Case 1 from [21] (1 to 5 blockage events per beam) and simulation was used as outlined in Table VI. However, in Case 2 the transmit power was evenly split between the two BSs for fairness, such that each TX transmitted 27 dBm of power for a combined overall transmit power of 30 dBm. Additionally, because the measurements used narrowbeam TX/RX antennas (7°/15°), blockers among separate beams are considered independent, especially when T-R separation distances are more than 20 meters (all cases in measurements), based on observations of short spatial correlation distances presented in [41].

At the receiver, three techniques were used to calculate the received power and the effective SNR and outage through diversity, where each RX beam points to and communicates with only 1 TX (forced diversity). The three diversity techniques include: selection diversity (SD) [6], equal gain combining (EGC), and maximum ratio combining (MRC). Each of the

TABLE VII: Single BS CDF of user SNR values (in dB) with and without human blockage events at 73 GHz (see Fig. 4a).

CDF of SNR Values for Blockage w/ One Base Station		
No. of TX / blockage?	-5 dB SNR Thresh. %	5% SNR
1 TX: no blockage	16.5%	-10.8 dB
1 TX: blockage	24.7%	-17.7 dB

three diversity techniques here can be associated with macro-diversity transmission or joint transmission in downlink CoMP with CSI shared between BSs [6], [15], [38].

3) Case 3: Three Base Stations: There were 42 combinations with 3 common TX locations to 1 RX location from the BS diversity measurements. Similar to Case 2, in Case 3 it was assumed that the RX could form 3 analog RF beams simultaneously for receiving and combining signals from three serving BSs, as depicted by the sketch in Fig 3. Again, we note that BS diversity is forced. By considering the 100 strongest beams from the measurement layout shown in Fig. 1 between each TX and the RX, 42×100^3 possible user received power beam combinations (*data points*) for 3 TXs to one RX were used. Human blockage events were simulated as in Case 2, and the transmit power was equally divided between the three BSs such that each transmitted 25.2 dBm of power (30 dBm combined).

B. Results and Analysis

1) Case 1: One Base Station Serving a Single User: Fig. 4a displays the CDF of single user SNRs in the presence of blockage events (red line) compared to the CDF of single user SNRs with no blockage events (blue line), for all single BS 36×100 received power data points from the measurements. The results in Fig. 4a exemplify the user SNRs expected in a typical mmWave UMi downlink scenario for T-R separation distances that range from 20.6 m to 169.9 m. Table VII provides details from the CDFs on outage with a -5 dB SNR threshold [42] and the 5% CDF points for SNR levels in dB. The CDFs in Fig. 4a reveal that 16.5% of users will experience an outage (-5 dB SNR threshold) with the system parameters specified in Table VI. In the presence of blockage events, SNR at a user degrades, where outage probability increases to 24.7%. Fig. 4a and Table VII also show that 5% of users experience a -10.8 dB SNR or worse without a blockage event, but that 5% of users experience -17.7 dB SNR in the presence of blockage events. The increase in outage and signal degradation with blockage events is significant in the mmWave regime and motivates the use of multiple BSs and user beams so that a user can maintain sufficient received signal level.

2) Case 2: Two Base Stations Serving a Single User: Using two BSs to serve a user during blockage events results in significant SNR improvements when using SD, EGC, and MRC at the user, as compared to a single BS. Fig. 4a shows the typical user SNRs with and without blockage events when served by two BSs for SD and MRC at the receiver, and Table VIII highlights the coverage and SNR improvements for the three diversity techniques of SD, EGC, and MRC.

Without human blockage events, results for 2 BSs with SD at the user show that 7.3% of users experience outage, compared to 16.5% when served by 1 BS. The probability of
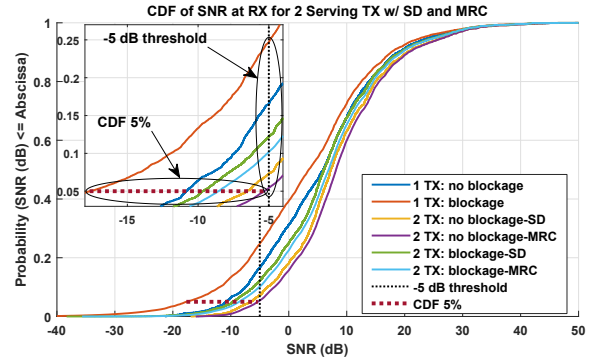
(a) Two BSs compared to one BS.
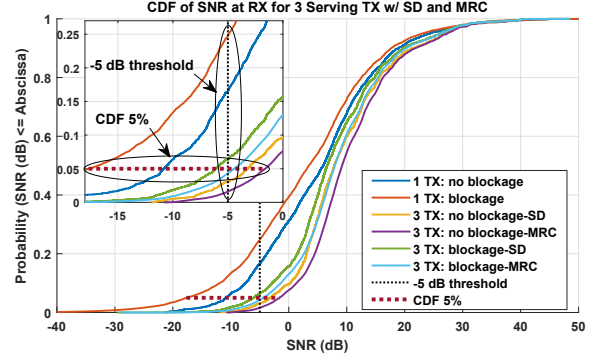
(b) Three BSs compared to one BS.

Fig. 4: CDF of user SNRs for diversity when served by (a) two and (b) three BSs using SD and MRC techniques at the receiver, with and without human blockage events at 73 GHz. The (a) two and (b) three beams at the user each come from a separate BS.

TABLE VIII: CDF of user SNR values for diversity at 73 GHz with two (three) serving BSs using SD, EGC, and MRC at the receiver (see Figs. 4a and 4b). The two (three) beams at the user each come from a separate BS.

CDF of SNR Values for Blockage w/ 2 Base Station Diversity		
No. of TX / blockage?	-5 dB SNR Thresh. %	5% SNR
2 TX-SD: no blockage	7.3%	-6.6 dB
2 TX-EGC: no blockage	6.6%	-6.0 dB
2 TX-MRC: no blockage	5.4%	-5.3 dB
2 TX-SD: blockage	12.2%	-9.7 dB
2 TX-EGC: blockage	12.2%	-9.4 dB
2 TX-MRC: blockage	10.2%	-8.6 dB
CDF of SNR Values for Blockage w/ 3 Base Stations		
No. of TX / blockage?	-5 dB SNR Thresh. %	5% SNR
3 TX-SD: no blockage	3.0%	-3.2 dB
3 TX-EGC: no blockage	2.4%	-2.9 dB
3 TX-MRC: no blockage	1.6%	-1.6 dB
3 TX-SD: blockage	6.3%	-6.1 dB
3 TX-EGC: blockage	6.2%	-5.8 dB
3 TX-MRC: blockage	4.3%	-4.4 dB

outage reduces more for EGC and MRC which are 6.6% and 5.4%, respectively, without blockage events. When random blockage events were simulated on each of the 2 TX beams to a user from two different BSs, the outage probability for SD, EGC, and MRC were lower than outage with a single BS, showing the significant improvements of using BS diversity with directional beams at mmWave. With coordinated joint transmission in the downlink and for each of the three diversity techniques, the 5% SNR CDF point has an improvement of 8 dB or more compared to the single BS case with blockage.

3) Case 3: Three Base Stations Serving a Single User: Fig. 4b plots the user SNR CDFs when employing SD and

MRC, for diversity with three BSs. We note in this case that the user can form three beams, one each to a separate BS as depicted in Fig. 3. Table VIII provides the -5 dB SNR threshold outage probabilities and 5% CDF point SNR values. As expected, outage probabilities are reduced as compared to users served by one or two BSs. In particular, as shown in Fig 4b and Table VIII, the probability of outage without blockage events by a user served by three BSs is 6.3%, 6.2% and 4.3% for SD, EGC, and MRC, respectively. The low probabilities of outage in the absence of blockers are a 10% or more improvement as compared to a user with a single serving BS where the probability of outage was 16.5%.

Using three serving BSs compared to two serving BSs in the presence of human blockers reduces the outage probability by nearly a half when the receiver employs SD or EGC diversity, and even more so for MRC where outage is reduced to 4.3% for three serving BSs compared to 10.2% for two serving BS, as shown in Tables VIII and VIII. Furthermore, results in Table VIII show that only 5% of user beams with three serving BSs will experience an SNR less than -4.4 dB when using MRC at the RX. Future mmWave networks will likely operate with multiple and directional beams from separate BSs serving a user in order to mitigate rapid fading events, where coordination via local and edge rapid re-routing techniques could be used to reliably serve a user under such conditions in a UMi at mmWave [37]. While using more BSs improves user coverage, this comes at the cost of additional network overhead. Work in [43] showed that multi-cell cooperation with two cells and dynamic clustering resulted in better network performance compared to static cells with larger clusters that had diminishing gains. Given the law of diminishing returns beyond $n = 3$, it is likely that more BSs beyond three at mmWave would result in diminishing gains for CoMP and link reliability, not to mention the increased network complexities [43].

VI. COORDINATED MULTIPOINT FOR INTERFERENCE SUPPRESSION

Coordinated multipoint (CoMP) techniques have been extensively studied in simulation and through field trials to implement CoMP in current 4G and LTE-A networks [38], [44], [45]. While CoMP consists of numerous techniques and goals, one is suppressing downlink interference, although 4G and LTE have had difficulties with such implementations due to inaccuracies in CSI, and due to backhaul requirements. CoMP networks require extremely synchronized coordination with accurate and up-to-date CSI shared between BSs. Network latencies and out-of-date CSI information cause serious issues when attempting to implement CoMP in practical scenarios [46]. Recently, simulations using mmWave channel models and ray-tracers have been used to study multicell cooperation for future mmWave networks [47], [48]. However, there have been few measurement studies on CoMP or multipoint transmission at mmWave [17], [18], nor have there been measurement based studies on the interference effects of coordination in realistic environments. Therefore, we used the 73 GHz mmWave UMi BS diversity measurements to study downlink CoMP with downlink precoding.

A. Problem Formulation and System Model

In a majority of CoMP simulations in the literature, fully digital TX and RX architectures are considered, but it is likely that mmWave systems will employ hybrid analog / digital architectures as a trade-off for lower power consumption. Moreover, future mmWave BSs for 5G are predicted to be made up of large antenna arrays where RF chains are connected to subsets of the antenna array known as subarrays, which can broadcast independent streams. Similarly, a mobile may have multiple antenna subarrays each with an RF chain to form independent analog RF beams / streams.

Throughout this section, the following notation is used: $\mathcal{A}$ is a set, $\mathbf{A}$ is a matrix, $\mathbf{a}$ is a vector, and a is a scalar. The Frobenius norm of $\mathbf{A}$ is denoted as $||A||_F$, while $\mathbf{A}^H$, $\mathbf{A}^T$, $\mathbf{A}^{-1}$, $\text{diag}(\mathbf{A})$, and $\text{Tr}(\mathbf{A})$ are its Hermitian (complex conjugate) transpose, transpose, inverse, diagonal, and trace, respectively. Here, the problem formulation and system model is for a general CoMP case as it relates to the BS diversity measurements, with the notion that each subarray structure on the BS or UE can perform analog beamforming and that each subarray is connected to a separate RF chain to baseband for a separate stream as part of a hybrid beamforming (HB) architecture. In our analysis we assume that there are M BSs each equipped with N_{BS} antenna subarrays that are each connected to an RF chain for independent streams via RF analog beamforming. Thus, each BS has a large antenna array made up of N_{BS} tiled subarrays, for $M \times N_{\text{BS}}$ total streams in the network. There are K users (or UEs) that are each equipped with N_{UE} antenna arrays that are each connected to an RF chain for independent streams via RF analog beamforming, similar to the BS, where N_{UE} is generally smaller than N_{BS}. Note that $M \times N_{\text{BS}} = K \times N_{\text{UE}}$ for our analysis. For each user k with $k \in \{1, ..., K\}$ having N_{UE} antenna arrays (streams), and each BS m with $m \in \{1, ..., M\}$ having N_{BS} subarrays (streams), the received signal vector, $\mathbf{y} \in \mathbb{C}^{K N_{\text{UE}} \times 1}$ for all $K \times N_{\text{UE}}$ streams across the entire network is expressed as:

$$\mathbf{y} = \sqrt{G_{RX}}\mathbf{H}\mathbf{W}\sqrt{G_{TX}}\sqrt{P_t}\mathbf{s} + \mathbf{n} \qquad (9)$$

where $\mathbf{H} \in \mathbb{C}^{K N_{\text{UE}} \times M N_{\text{BS}}}$ is the network-wide channel matrix, $\mathbf{W} \in \mathbb{C}^{M N_{\text{BS}} \times K N_{\text{UE}}}$ is the linear baseband precoding matrix, $\mathbf{s} \in \mathbb{C}^{K N_{\text{UE}} \times 1}$ is the transmit symbol vector, and $\mathbf{n} \in \mathbb{C}^{K N_{\text{UE}} \times 1}$ is the noise vector [49]. G_{TX} and G_{RX} are the linear antenna gains at all BS and user subarrays, respectively, and P_t is the average transmit power fed into each BS subarray. Translated to a typical system model, $\sqrt{G_{TX}}$, the main beam boresight, in the best direction for maximum SNR, may be considered as the best RF analog precoder W_{RF}, and $\sqrt{G_{RX}}$ may be considered as the best RF analog combiner F_{RF}.

The network-wide $K N_{\text{UE}} \times M N_{\text{BS}}$ channel matrix $\mathbf{H}$ in (9) is formed as $\mathbf{H} = \begin{bmatrix} \mathbf{H}_1^T, ..., \mathbf{H}_K^T \end{bmatrix}^T$, where $\mathbf{H}_k = \begin{bmatrix} \mathbf{h}_{k,i}^T, ..., \mathbf{h}_{k,N_{\text{UE}}}^T \end{bmatrix}^T \in \mathbb{C}^{N_{\text{UE}} \times M N_{\text{BS}}}$ is the channel matrix between all BS subarrays and user k [49]. $\mathbf{h}_{k,i} \in \mathbb{C}^{1 \times M N_{\text{BS}}}$ denotes the channel vector between all BS subarrays and the user k's i-th subarray (stream). The network-wide $M N_{\text{BS}} \times K N_{\text{UE}}$ baseband linear precoding matrix $\mathbf{W}$ is defined as $\mathbf{W} = [\mathbf{W}_1, ..., \mathbf{W}_K]$, where $\mathbf{W}_k = [\mathbf{w}_{k,1}, ..., \mathbf{w}_{k,N_{\text{UE}}}] \in \mathbb{C}^{M N_{\text{BS}} \times N_{\text{UE}}}$ is the precoding matrix jointly used across all

BSs for transmitting streams to user k, and $\mathbf{w}_{k,i} \in \mathbb{C}^{M\,N_{\text{BS}}\times 1}$ is the precoding vector for stream (subarray) i. Transmit symbol vector $\mathbf{s}$ is defined as $\mathbf{s} = \left[\mathbf{s}_1^T, ..., \mathbf{s}_K^T\right]^T$, with $\mathbf{s}_k = \left[s_{k,1}, ..., s_{k,N_{\text{UE}}}\right]^T$, where $s_{k,i}$ denotes the transmit symbol of stream (subarray) i for user k, and $\mathbb{E}[s_{i,k}s_{i,k}^H] = 1$ for all i and k. Similarly, the noise vector $\mathbf{n}$ is expressed as $\mathbf{n} = \left[\mathbf{n}_1^T, ..., \mathbf{n}_K^T\right]^T$, where $\mathbf{n}_k = [n_{k,1}, ..., n_{k,N_{\text{UE}}}]^T$ denotes the noise vector at user k, and $n_{k,i} \sim \mathcal{CN}(0, \sigma_n^2)$. The noise variance σ_n^2 includes thermal noise power N_0 and any additional noise power. To simplify (9), the received signal vector, $\mathbf{y}_k \in \mathbb{C}^{N_{\text{UE}}\times 1}$ at the k-th user is written as:

$$\mathbf{y}_k = \sqrt{G_{RX}}\mathbf{H}_k\mathbf{W}_k\sqrt{G_{TX}}\sqrt{P_t}\mathbf{s}_k$$
$$+ \sqrt{G_{RX}}\mathbf{H}_k\sum_{l=1,l\neq k}^{K}\mathbf{W}_l\sqrt{G_{TX}}\sqrt{P_t}\mathbf{s}_l + \mathbf{n}_k \quad (10)$$

We now further decompose (10) to show the received signal, $y_{k,i} \in \mathbb{C}^{1\times 1}$ of the i-th stream for the k-th user:

$$y_{k,i} = \sqrt{G_{RX}}\sqrt{G_{TX}}\sqrt{P_t}\Bigg[\underbrace{\mathbf{h}_{k,i}\mathbf{w}_{k,i}s_{k,i}}_{\text{Desired Signal}}$$
$$+ \underbrace{\sum_{l=1,l\neq i}^{N_{\text{UE}}}\mathbf{h}_{k,i}\mathbf{w}_{k,l}s_{k,l}}_{\text{Intracell Interference}} + \underbrace{\sum_{j=1,j\neq k}^{K}\sum_{l=1}^{N_{\text{UE}}}\mathbf{h}_{k,i}\mathbf{w}_{j,l}s_{j,l}}_{\text{Intercell Interference}}\Bigg] + \underbrace{n_{k,i}}_{\text{Noise}}$$
$$(11)$$

In the analysis we assume perfect network synchronization, and perfect CSI is known and shared with all BSs connected to a central unit (CU) via high-speed backhaul in order to implement coordinating scheduling and coordinated beamforming (CS/CB) in the downlink with network precoding [50], and ignore human blockage. To eliminate interference in the network, zero-forcing (ZF) precoding is used by multiplying the network channel $\mathbf{H}$ by its pseudoinverse [13], [51]: $\mathbf{W}_{\text{ZF}} = \mathbf{H}^H(\mathbf{H}\mathbf{H}^H)^{-1}$. Zero-forcing precoding works by eliminating the intracell and intercell interference in (11), although it ignores additive Gaussian noise and can inflate noise power in low SNR conditions [51]. Another precoding approach, matched filtering (MF), is used to maximize the SNR of each stream to all K users by multiplying the network channel by its conjugate [51]: $\mathbf{W}_{\text{MF}} = \mathbf{H}^H$. MF essentially maximizes the desired signal power in (11) and works well in low SNR regimes since it maximizes signal power but performs poorly in high SNR regimes since it disregards inter-stream and inter-user interference. The MMSE precoder is nearly identical in form to the ZF precoder, yields significantly better performance at low SNR compared to ZF, and better performance at high SNR compared to MF. Essentially, the MMSE precoder performance converges to that of MF precoding in the low SNR regime and to ZF precoding in the high SNR regime. The MMSE precoding filter is expressed as [51], [52]: $\mathbf{W}_{\text{MMSE}} = \mathbf{H}^H(\mathbf{H}\mathbf{H}^H + \alpha\mathbf{I})^{-1}$, where α is a regularization factor that is commonly chosen to be $\alpha = K \times N_{\text{UE}}\,\sigma_n^2/P_t$, and has been shown to approximately maximize the receive SINR [51], [53]. In order to satisfy the power constraint for all precoders such that the total transmit power P_{total} across all $M \times N_{\text{BS}}$ BS subarrays does not exceed

$P_t \times M \times N_{\text{BS}}$, we normalize the transmit precoding vectors $\mathbf{w}_{k,i}$ as $\tilde{\mathbf{w}}_{k,i} \triangleq \mathbf{w}_{k,i}/(\sqrt{M\,N_{\text{BS}}}\,||\mathbf{w}_{k,i}||_F^2)$. Using (11), we now express the SINR of the i-th stream for the k-th user as in (13), where the network spectral efficiency is given by

$$R = \sum_{k=1}^{K}R_k = \sum_{k=1}^{K}\sum_{i=1}^{N_{\text{UE}}}\log_2\left(1 + \text{SINR}_{k,i}\right) \quad (12)$$

The problem formulation and system setup described in this subsection is subsequently used with the BS diversity measurements.

B. Relation Between Measurements and Problem Formulation

Per the BS diversity measurements outlined in Section II-B, each single TX-RX location combination included PDP measurements for 15 TX AODs and up to 72 AOAs, per AOD. For analysis purposes, we consider the 15 AODs with the horn antenna gain of G_{TX} to be akin to an RF precoder W_{RF} for each BS subarray. Similarly, we consider the AOAs with the horn antenna gain of G_{RX} to mimic an RF combiner F_{RF} for each user subarray. Considering the horn antennas as subarrays allows us to consider multiple pointing beams between each TX and RX. We use the average channel gain across a frequency-flat fading channel of 1 GHz (like OFDM with flat-fading sub-carriers). By removing antenna gains from the directional measurements, the channel gain magnitude h is determined by taking the square-root of the ratio of the received power to the transmit power: $h = \sqrt{P_r/P_t}$. Since the measurements did not offer phase information, a random phase $\theta \sim U(-\pi, \pi)$, was applied to each channel coefficient h [7], [23]. deterministically [7], [23].

We define a CoMP network setting with $M = 2$, $K = 2$, $N_{\text{BS}} = 1$ and $N_{\text{UE}} = 1$, by choosing a set of 2 common TXs and 2 common RXs from the measurements (see Section II), such that each BS and user is equipped with a single subarray connected to one RF chain, resulting in a 2×2 network-wide channel matrix $\mathbf{H}$, where the diagonal elements denote the channel coefficients between the assigned BS-user pairs, and the off-diagonal elements denote the interfering channel coefficients, as sketched in Fig. 5. The measurement campaign resulted in 34 CoMP network settings of 2 common TXs to 2 common RXs (see Section II-C). We assign one TX to one RX, and then swap the TX to RX assignment to extend the total CoMP network settings to $2 \times 34 = 68$, for analysis. In order to analyze a large number of CoMP network settings, the 100 best beams (lowest path loss) between each TX to RX assignment were used, resulting in 68×100^2 *CoMP networks or network settings* from the measurement campaign. Of the 68×100^2 CoMP network settings from the BS diversity measurements, 43% resulted in off-diagonal elements of 0, i.e., $h_{1,2} = h_{2,1} = 0$, indicating that the two RXs for 43% of the CoMP networks did not experience interference. The analysis parameters are specified in Table IX, where the BS and user subarray gains are set to 27 dBi, and 20 dBi, respectively, as those were the gains of the measurement antennas (see Section II). Note, we assume each TX and RX only employ one subarray which is essentially a single array at each TX and RX. Thus, the TX and RX are only able to form 1 beam

$$\text{SINR}_{k,i} = \frac{G_{RX}G_{TX}P_t|\mathbf{h}_{k,i}\tilde{\mathbf{w}}_{k,i}|^2}{G_{RX}G_{TX}P_t\sum_{l=1,l\neq i}^{N_{\text{UE}}}|\mathbf{h}_{k,i}\tilde{\mathbf{w}}_{k,l}|^2 + G_{RX}G_{TX}P_t\sum_{j=1,j\neq k}^{K}\sum_{l=1}^{N_{\text{UE}}}|\mathbf{h}_{k,i}\tilde{\mathbf{w}}_{j,l}|^2 + \sigma_n^2} \quad (13)$$

TABLE IX: Parameter settings for CoMP analysis using the BS diversity measurements at 73 GHz.

| Parameter	Setting
Carrier Frequency	73.5 GHz
Bandwidth	1 GHz
Number of BS	$M = 2$
Antenna Arrays per BS	$N_{\text{BS}} = 1$
Number of Users	$M = 2$
Antenna Arrays per User	$N_{\text{UE}} = 1$
Gain per BS Antenna Array	27 dBi
Average Transmit Power per BS Antenna Array	30 dBm
Gain per User Antenna Array	20 dBi
Max Measurable Path Loss	175 dB
Thermal Noise Power N_0	-84 dBm
User Noise Figure	10 dB
TX / RX Polarization	V / V
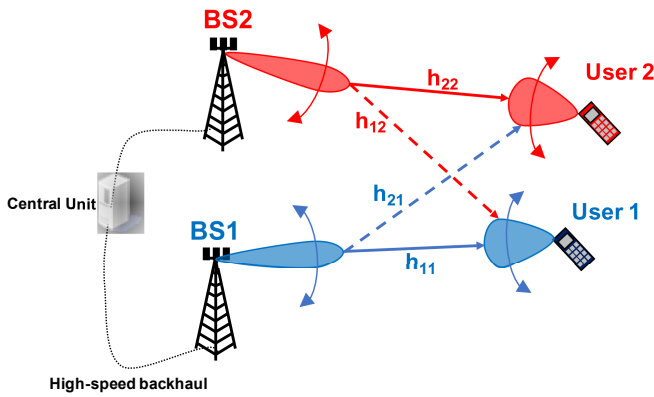
Fig. 5: Sketch of a 2×2 CoMP network setting, with a single subarray/RF chain at each BS and user. CSI is available at all BSs and the CU via high-speed backhaul for joint processing and CS/CB for CoMP downlink precoding.

(a)

(b)

Fig. 6: 2×2 CoMP networks with full-interference at 73 GHz, for CDF of a) per-user SINR; b) network spectral efficiency.

each at a time. The average transmit power P_t per subarray at each BS is set to 30 dBm, the noise figure at each user RF chain (one per user) is set to 10 dB, with thermal noise power $N_0 = -84$ dBm across 1 GHz of bandwidth. We note that results here are an aggregation of real-world measurement data with the simulation parameters in Table IX.

C. Results and Analysis

As described above, not all of the $68 \times 100^2 = 680,000$ CoMP network settings resulted interference for one or both of the RX beams. The lack of interference is expected due to the use of directional beams in mmWave systems, which are typically noise-limited rather than interference-limited [2]. As a result, only 22% of all the 68×100^2 CoMP network settings have both interfering signals (e.g. TX1 to RX2 and TX2 to RX1), referred to as *full-interference*. Subsequently, 35% of the CoMP network settings have only one interfering signal (e.g. only interference from TX1 to RX2 or TX2 to RX1), referred to as *partial-interference*. Furthermore, there were no interfering signals observed in 43% of the 68×100^2 CoMP network settings, referred to as *no-interference*.

1) Full-Interference CoMP Network Setting: Fig. 6a shows user SINR CDFs for no coordination (uncoordinated), and
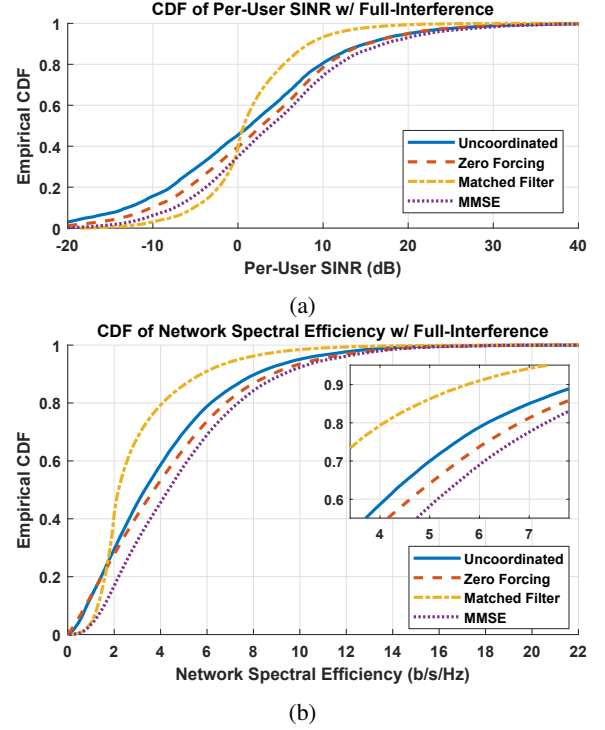
downlink precoding with ZF, MF, and MMSE. Table X gives the 10%, 50% and 90% CDF points of user SINR in dB, user spectral efficiency (SE) in b/s/Hz, and network SE in b/s/Hz. Fig. 6a shows that MF precoding suppresses the interference experienced by the users such that the range of SINR across all network users is reduced compared to the ZF and MMSE cases, which in turn limits the overall performance in terms of spectral efficiency. The reduction in the range of user SINRs with MF is specifically noticed in Table X, where the 10% to 90% SINRs range from -5.2 dB to 8.3 dB, respectively, compared to uncoordinated that ranges from -13.4 dB to 15.0, respectively. With no coordination, 10% of the users experience -13.4 dB SINR or less, however, with downlink precoding and network coordination, the 10% CDF point improves by 3.2 dB with ZF, by 5.9 dB with MMSE and by 8.2 dB with MF. Even though MF results in a higher 10% SINR CDF point (e.g. better user SINR improvement in low SNR conditions) compared to ZF and MMSE, the MF 90% CDF point is much worse than ZF and MMSE due to high SNR conditions from the 100 best beam combinations. Since we used the best 100 beams from each individual TX-RX combination from the measurements, higher SNR conditions are more likely, hence, MF is not desirable. The network spectral efficiencies, displayed in Fig 6b illustrate the superiority of ZF compared to MF, given that the system is operating in high SNR, due to mmWave beamforming.

TABLE X: CDF points of 2×2 CoMP networks with full-interference at 73 GHz, for i) per-user SINR in dB, ii) per-user spectral efficiency in b/s/Hz, and iii) network spectral efficiency in b/s/Hz.

CoMP Setting CDF Statistics for Full-Interference			
CDF %	UC	MF	ZF	MMSE
Per-User SINR in dB			
10%	-13.4	-5.2	-10.2	-7.5
50%	1.4	0.7	2.8	3.9
90%	15.0	8.3	15.2	17.2
Per-User Spectral Efficiency in b/s/Hz			
10%	0.08	0.4	0.1	0.2
50%	1.3	1.1	1.5	1.8
90%	5.0	3.0	5.1	5.7
Network Spectral Efficiency in b/s/Hz			
10%	0.8	1.3	0.8	1.6
50%	3.3	2.2	3.7	4.3
90%	8.1	5.8	8.8	9.3

TABLE XI: CDF points of 2×2 CoMP networks with partial-interference at 73 GHz, for i) per-user SINR in dB, ii) per-user spectral efficiency in b/s/Hz, and iii) network spectral efficiency in b/s/Hz.

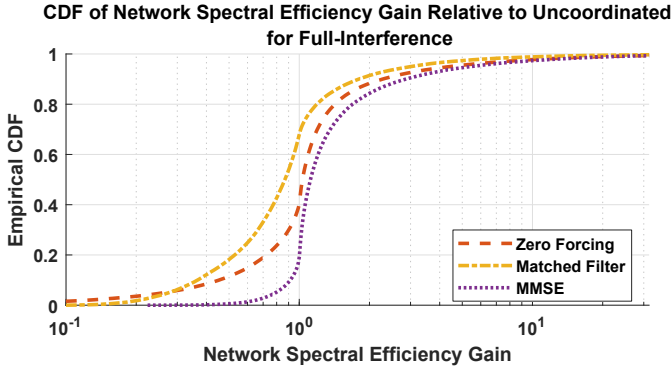| CoMP Setting CDF Statistics for Partial-Interference			
CDF %	UC	MF	ZF	MMSE
Per-User SINR in dB			
10%	-12.7	-8.6	-13.4	-10.0
50%	3.0	1.6	3.1	3.8
90%	16.0	12.8	16.1	16.7
Per-User Spectral Efficiency in b/s/Hz			
10%	0.08	0.2	0.06	0.14
50%	1.6	1.3	1.6	1.8
90%	5.3	4.3	5.4	5.6
Network Spectral Efficiency in b/s/Hz			
10%	0.8	1.0	0.6	1.1
50%	3.8	3.0	3.9	4.1
90%	8.9	8.0	9.1	9.3

Fig. 7: CDF of network spectral efficiency gain relative to the uncoordinated case for full-interference.

MF and MMSE are shown to increase the low performing networks in Fig. 6b at the 10% point to 1.3 b/s/Hz and 1.6 b/s/Hz, respectively, compared to 0.8 b/s/Hz for the uncoordinated case. Most notably though, ZF and MMSE precoding improve a majority of network spectral efficiencies as shown in Fig. 6b, especially at the 90% point with values of 8.8 b/s/Hz and 9.3 b/s/Hz, respectively, compared to UC and MF that have 90% points of 8.1 b/s/Hz, and 5.8 b/s/Hz, respectively. MF performance is lower than UC at the 90% point, due to the fact that MF increases both the signal strength and interference, which reduces performance when SNR is high (beamforming applied).

Fig. 7 displays the CDF of the network spectral efficiency normalized to the uncoordinated case. For MF and ZF, approximately 40% and 65% of the CoMP network settings with full-interference do not show a gain in overall network spectral efficiency, respectively, compared to uncoordinated. However, 81% of the CoMP network settings show a gain when using MMSE precoding. The under-performance of 19% of the full-interference CoMP network settings with MMSE is due to the fixed (conventional) choice of the regularization factor α for MMSE, resulting in network spectral efficiencies to gravitate towards the suboptimal strategies of MF or ZF.

2) Partial-Interference CoMP Network Setting: The user SINR CDFs with and without CoMP network coordination for the partial-interference CoMP networks (only one user experiences interference) are shown in Fig. 8a. Compared to the full-interference CoMP networks, the user SINRs for partial-interference show smaller improvements with coordi-

nation. For example, Table XI provides the CDF points of per-user SINRs and shows that MF improves the 10% per-user SINR point from -12.7 dB and to -8.6 dB compared to uncoordinated. Like the full-interference CoMP networks described in the previous subsection, MF performs worse in high SNR conditions as noticed by the 90% point per-user SINRs of 12.8 dB for MF in Table XI compared to 16.1 dB and 16.7 dB for ZF and MMSE, respectively. Since only one of the two users experiences interference, the 50% per-user SINR point is within 2 dB or so for the uncoordinated case and all coordinated cases, meaning that median per-user SINRs see little to no improvement with downlink precoding for partial interference.

Fig. 8b plots the CDFs of network spectral efficiencies and shows the superiority of ZF and especially MMSE. Across all respective CDF points (10%, 50%, and 90%), there is no more than approximately 1 b/s/Hz difference among the uncoordinated (no network coordination and no downlink precoding) and the three coordinated precoding cases. While coordinated precoding does improve the overall network spectral efficiency compared to no coordination, it is apparent that the improvement is much less significant compared to the full-interference case, where the 90% CDF points of network spectral efficiency with partial-interference are 8.9 b/s/Hz and 9.3 b/s/Hz for UC and MMSE, respectively, compared to 8.1 b/s/Hz and 9.3 b/s/Hz for the full-interference case. The reason for this observation is the fact that not all users in the network experience interference, thus, the overall improvements are less for the partial interference case. The CDF of network spectral efficiency gains for partial interference are displayed in Fig. 9 and show that coordination gains are less compared to the full-interference case. While MMSE shows that 81% of the CoMP networks experience a gain compared to uncoordinated networks, only 7% of the networks for the partial-interference case achieve a gain of 2 or better compared to 16% for the full-interference CoMP networks with MMSE.

3) No-Interference CoMP Network Setting: Although performance cannot be improved with downlink CoMP when no-interference is present, the SNR CDF results for the 43% of CoMP networks with no-interference are provided in Table XII to show the typical performance. An interesting result here is that only 13% of users in the CoMP network settings with no-interference have an SINR of -5 dB or lower, showing that
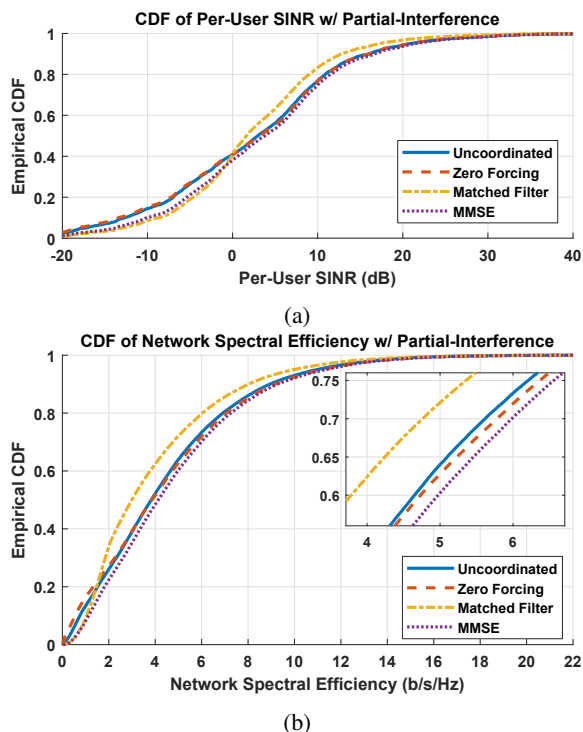
(a)

(b)

Fig. 8: 2×2 CoMP networks with partial-interference at 73 GHz, for CDF of a) per-user SINR; b) network spectral efficiency.

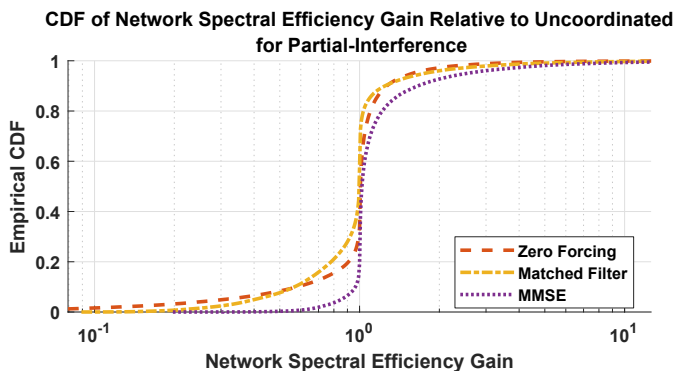Fig. 9: CDF of network spectral efficiency gain relative to the uncoordinated case for partial-interference.

TABLE XII: CDF points of 2×2 CoMP networks with no-interference at 73 GHz, for i) per-user SINR in dB, ii) per-user spectral efficiency in b/s/Hz, and iii) network spectral efficiency in b/s/Hz.

CoMP Setting CDF Statistics for No-Interference	
CDF %	Per-User SINR in dB
10%	-6.1
50%	7.9
90%	19.8
CDF %	Per-User Spectral Efficiency in b/s/Hz
10%	0.3
50%	2.8
90%	6.6
CDF %	Network Spectral Efficiency in b/s/Hz
10%	2.4
50%	5.8
90%	11.6

it induces an accumulation of estimation errors [54]. Thus, it is expected that the network performance results presented here for CoMP at mmWave would also degrade with imperfect CSI for interference and no-interference scenarios. Even with perfect CSI, the results here show how site-specific deployments used with directional antennas at mmWave could remove the need for downlink coordination and the exchange of CSI between BSs, at least for interference suppression. Thus, the use of narrowbeam antennas at mmWave could render downlink interference mitigation unnecessary. However, we note that the results presented here are strictly based on the CoMP network deployment shown in Fig. 1.

VII. CONCLUSION

In this paper, we presented an extensive 73 GHz mmWave BS diversity measurement campaign with directional TX and RX antennas that resulted in more than 130 Gigabytes of data and that included more than 26,000 directional PDPs across numerous locations and AODs and AOAs, that were used for modeling and analysis. The LOS-B and NLOS-Best directional PLEs of 2.0 and 3.1, respectively, indicate favorable propagation characteristics in LOS and NLOS UMi scenarios when TX and RX antennas can optimally align their beams. Hypothesis testing and cross-validation with directional shadow fading measurements showed that shadow fading between the two and three nearest neighbor BSs and an RX can be modeled as independent (uncorrelated) Gaussian. Furthermore, attenuation from multiple simulated human blockage event traces were superimposed on real-world directional beam received power from the BS diversity measurements, and analysis showed that the percentage of users in outage is reduced to 10.2% and 4.3% when using two and three BSs to serve a user, respectively, as compared to 24.7% when served by one BS. Therefore, the use of rapid re-routing techniques will be helpful in mitigating user outages in mmWave UMi scenarios [37]. Finally, while downlink CoMP network coordination with CSI at BSs was shown to improve network performance when interference is present, this was only the case for 22% of the CoMP networks analyzed (full-interference), whereas network precoding had minimal gain for partial-interference, and no gain as expected, when interference was not present for 43% of the 680,000 CoMP networks analyzed. What this reveals

nearly 87% of the users (from the deployment in Fig. 1) will likely not experience an outage when a threshold of -5 dB SINR is used, meaning that less stringent requirements for downlink interference cooperation could be used for CoMP networks at mmWave. The network spectral efficiency 90% point in Table XII is higher for no-interference at 11.6 b/s/Hz, compared to MMSE network precoding for full- and partial-interference which are both 9.3 b/s/Hz.

The observations here beg one to consider whether or not the resources needed for CoMP for interference suppression are necessary when nearly half ($\sim 43\%$) of the CoMP networks result in no interference to either user. Moreover, we considered networks with perfect CSI. Studies on CoMP interference mitigation for LTE networks showed that imperfect channel estimation leads to significant degradation of network performance, especially as the number of BSs increases since

is that when BSs and users align their narrow and directional beams, the interference to neighboring BS-user assignments is quite minimal. Even in the scenario with full-interference, 50% of networks achieve 1 b/s/Hz improvement compared to uncoordinated beams. Therefore, the small performance gains from interference mitigation achieved by CoMP for networks analyzed herein, may not be worth the sharing of full CSI and coordination between BSs, which requires enormous backhaul overhead and stringent synchronization, while macrodiversity techniques to combat human blockage and rapid fading show more favorable improvements. Future work to extend the work herein will explore the use of frequencies above 95 GHz which may someday support 6G [55], along with enhancing the NYUSIM channel simulator by incorporating the shadowing and human blockage model of pedestrians over a local area based on spatial consistency [56].

REFERENCES

[1] International Telecommunications Union, "IMT vision framework and overall objectives of the future development of IMT for 2020 and beyond," Geneva, Switzerland, Rec. ITU-R M.2083, Sept. 2015.

[2] T. S. Rappaport et al., "Millimeter Wave Mobile Communications for 5G Cellular: It Will Work!" IEEE Access, vol. 1, pp. 335–349, May 2013.

[3] ——, "Wideband millimeter-wave propagation measurements and channel models for future wireless communication system design (Invited Paper)," IEEE Transactions on Communications, vol. 63, no. 9, pp. 3029–3056, Sept. 2015.

[4] Aalto University et al., "5G channel model for bands up to 100 GHz," 2016, Oct. 21. [Online]. Available: http://www.5gworkshops.com/5GCM.html

[5] Z. Pi and F. Khan, "An introduction to millimeter-wave mobile broadband systems," IEEE Communications Magazine, vol. 49, no. 6, pp. 101–107, June 2011.

[6] M. Schwartz, W. R. Bennett, and S. Stein, Linear Diversity Combining Techniques. Wiley-IEEE Press, 1996.

[7] T. S. Rappaport, Wireless Communications, 2nd ed. Upper Saddle River, NJ: Prentice Hall, 2002.

[8] P. B. Papazian et al., "Study of the local multipoint distribution service radio channel," IEEE Transactions on Broadcasting, vol. 43, no. 2, pp. 175–184, June 1997.

[9] G. Hendrantoro, R. J. C. Bultitude, and D. D. Falconer, "Use of cell-site diversity in millimeter-wave fixed cellular systems to combat the effects of rain attenuation," IEEE J. Sel. Areas Commun., vol. 20, no. 3, pp. 602–614, Apr. 2002.

[10] S. Farahvash and M. Kavehrad, "Assessment of cochannel interference in fixed wireless cellular systems," in 1999 IEEE Radio and Wireless Conference (RAWCON 99), Aug. 1999, pp. 13–16.

[11] S. Q. Gong and D. Falconer, "Cochannel interference in cellular fixed broadband access systems with directional antennas," Wireless Personal Communications, vol. 10, no. 1, pp. 103–117, June 1999.

[12] H. V. Le et al., "Diversity property of millimeter wave wireless networks against localized rain," in 2014 IEEE Fifth International Conference on Communications and Electronics (ICCE), July 2014, pp. 407–410.

[13] M. K. Karakayali, G. J. Foschini, and R. A. Valenzuela, "Network coordination for spectrally efficient communications in cellular systems," IEEE Wireless Communications, vol. 13, no. 4, pp. 56–61, Aug. 2006.

[14] C.-X. Wang et al., "Cooperative MIMO channel models: A survey," IEEE Commun. Mag., vol. 48, no. 2, pp. 80–87, Feb. 2010.

[15] 3GPP, "Technical specification group radio access network; coordinated multi-point operation for LTE physical layer aspects (Release 11)," 3rd Generation Partnership Project (3GPP), TR 36.819, Sept. 2013.

[16] S. Sun et al., "Analytical framework of hybrid beamforming in multi-cell millimeter-wave systems," IEEE Transactions on Wireless Communications, vol. 17, no. 11, pp. 7528–7543, Nov. 2018.

[17] D. Kurita et al., "Field experiments on 5G radio access using multi-point transmission," in 2015 IEEE Global Telecommunications Conference Workshops (Globecom Workshops), Dec. 2015, pp. 1–6.

[18] B. Halvarsson et al., "Distributed mimo demonstrated with 5g radio access prototype," in 2016 European Conference on Networks and Communications (EuCNC), June 2016, pp. 302–306.

[19] D. Kurita et al., "Indoor and outdoor experiments on 5G radio access using distributed MIMO and beamforming in 15 GHz frequency band," in 2016 IEEE Globecom Workshops (GC Wkshps), Dec. 2016, pp. 1–6.

[20] G. R. MacCartney, Jr., "Millimeter-wave base station diversity and human blockage in dense urban environments for coordinated multipoint (comp) applications," Ph.D. dissertation, NYU, Tandon School of Engineering, May 2018.

[21] G. R. MacCartney, Jr., T. S. Rappaport, and S. Rangan, "Rapid fading due to human blockage in pedestrian crowds at 5g millimeter-wave frequencies," in 2017 IEEE Global Communications Conference (GLOBECOM), Dec. 2017, pp. 1–7.

[22] G. R. MacCartney, Jr., T. S. Rappaport, and A. Ghosh, "Base station diversity propagation measurements at 73 GHz millimeter-wave for 5G coordinated multipoint (CoMP) applications," in 2017 IEEE Globecom Workshops (GC Wkshps), Dec. 2017, pp. 1–7.

[23] G. R. MacCartney, Jr. and T. S. Rappaport, "A flexible millimeter-wave channel sounder with absolute timing," IEEE Journal on Selected Areas in Communications, vol. 35, no. 6, pp. 1402–1418, June 2017.

[24] S. Sun et al., "Investigation of prediction accuracy, sensitivity, and parameter stability of large-scale propagation path loss models for 5G wireless communications (Invited Paper)," IEEE Transactions on Vehicular Technology, vol. 65, no. 5, pp. 2843–2860, May 2016.

[25] G. R. MacCartney, Jr. et al., "Indoor office wideband millimeter-wave propagation measurements and models at 28 GHz and 73 GHz for ultra-dense 5G wireless networks (Invited Paper)," IEEE Access, vol. 3, pp. 2388–2424, Oct. 2015.

[26] T. S. Rappaport, R. W. Heath, Jr., R. C. Daniels, and J. N. Murdock, Millimeter Wave Wireless Communications. Pearson/Prentice Hall, 2015.

[27] H. T. Friis, "A note on a simple transmission formula," Proceedings of the IRE, vol. 34, no. 5, pp. 254–256, May 1946.

[28] V. Graziano, "Propagation correlations at 900 MHz," IEEE Trans. Veh. Technol., vol. 27, no. 4, pp. 182–189, Nov. 1978.

[29] K. Zayana and B. Guisnet, "Measurements and modelisation of shadowing cross-correlations between two base-stations," in IEEE 1998 International Conference on Universal Personal Communications, ICUPC '98., vol. 1, Oct. 1998, pp. 101–105.

[30] M. Gudmundson, "Correlation model for shadow fading in mobile radio systems," Electronics Letters, vol. 27, no. 23, pp. 2145–2146, Nov. 1991.

[31] S. Geisser, Predictive Inference. New York, NY: Chapman and Hall, 1995.

[32] C. G. Atkeson, A. W. Moore, and S. Schaal, "Locally weighted learning for control," Artificial Intelligence Review, vol. 11, no. 1, pp. 75–113, Feb 1997.

[33] R. Picard and D. Cook, "Cross-validation of regression models," Journal of the American Statistical Association, vol. 79, no. 387, pp. 575–583, 1984.

[34] G. James, D. Witten, T. Hastie, and R. Tibshirani, An Introduction to Statistical Learning. Springer, 2013.

[35] R. J. Weiler et al., "Environment induced shadowing of urban millimeter-wave access links," IEEE Wireless Communications Letters, vol. 5, no. 4, pp. 440–443, Aug. 2016.

[36] S. Singh et al., "Blockage and directivity in 60 GHz wireless personal area networks: from cross-layer model to multihop MAC design," IEEE Journal on Selected Areas in Communications, vol. 27, no. 8, pp. 1400–1413, Oct. 2009.

[37] A. Ghosh, "The 5G mmWave radio revolution," Microwave Journal, vol. 59, no. 9, pp. 22–36, Sept. 2016.

[38] D. Lee et al., "Coordinated multipoint transmission and reception in LTE-advanced: deployment scenarios and operational challenges," IEEE Communications Magazine, vol. 50, no. 2, pp. 148–155, Feb. 2012.

[39] V. Jungnickel et al., "The role of small cells, coordinated multipoint, and massive MIMO in 5G," IEEE Communications Magazine, vol. 52, no. 5, pp. 44–51, May 2014.

[40] 3GPP, "Technical specification group radio access network; study on channel model for frequencies from 0.5 to 100 GHz (Release 14)," 3rd Generation Partnership Project (3GPP), TR 38.901 V14.2.0, Sept. 2017.

[41] T. S. Rappaport et al., "Small-scale, local area, and transitional millimeter wave propagation for 5G communications," IEEE Transactions on Antennas and Propagation, vol. 65, no. 12, pp. 6474–6490, Dec. 2017.

[42] J. G. Andrews, F. Baccelli, and R. K. Ganti, "A tractable approach to coverage and rate in cellular networks," IEEE Transactions on Communications, vol. 59, no. 11, pp. 3122–3134, Nov. 2011.

[43] A. Papadogiannis, D. Gesbert, and E. Hardouin, "A dynamic clustering approach in wireless networks with multi-cell cooperative processing," in 2008 IEEE International Conference on Communications, May 2008, pp. 4033–4037.

[44] N. Jalden *et al.*, "Analysis of multi-cell mimo measurements in an urban macrocell environment," *General Assembly of International Union of Radio Science (URSI '05)*, pp. 1–12, Oct. 2005.

[45] K. Huang and J. G. Andrews, "An analytical framework for multicell cooperation via stochastic geometry and large deviations," *IEEE Transactions on Information Theory*, vol. 59, no. 4, pp. 2501–2516, Apr. 2013.

[46] R. W. Heath *et al.*, "An overview of signal processing techniques for millimeter wave mimo systems," *IEEE Journal of Selected Topics in Signal Processing*, vol. 10, no. 3, pp. 436–453, Apr. 2016.

[47] Z. Zhang *et al.*, "Coverage and channel characteristics of millimeter wave band using ray tracing," in *2015 IEEE International Conference on Communications (ICC)*, June 2015, pp. 1380–1385.

[48] D. Maamari, N. Devroye, and D. Tuninetti, "Coverage in mmWave cellular networks with base station co-operation," *IEEE Transactions on Wireless Communications*, vol. 15, no. 4, pp. 2981–2994, Apr. 2016.

[49] S. Park, A. Alkhateeb, and R. W. Heath, "Dynamic subarrays for hybrid precoding in wideband mmWave MIMO systems," *IEEE Transactions on Wireless Communications*, vol. 16, no. 5, pp. 2907–2920, May 2017.

[50] X. Li *et al.*, "A multi-cell MMSE precoder for massive MIMO systems and new large system analysis," in *2015 IEEE Global Communications Conference (GLOBECOM)*, Dec. 2015, pp. 1–6.

[51] C. B. Peel, B. M. Hochwald, and A. L. Swindlehurst, "A vector-perturbation technique for near-capacity multiantenna multiuser communication-part i: channel inversion and regularization," *IEEE Trans. Commun.*, vol. 53, no. 1, pp. 195–202, Jan. 2005.

[52] H. Huang, C. B. Papadias, and S. Venkatesan, *MIMO Communication for Cellular Networks*. Springer, 2012.

[53] F. Kaltenberger *et al.*, "Capacity of linear multi-user MIMO precoding schemes with measured channel data," in *2008 IEEE 9th Workshop on Signal Processing Advances in Wireless Communications*, July 2008, pp. 580–584.

[54] A. M. Hamza, J. W. Mark, and E. A. Sourour, "Interference analysis and mitigation for time-asynchronous OFDM CoMP systems," *IEEE Transactions on Wireless Communications*, vol. 17, no. 7, pp. 4780–4791, July 2018.

[55] Y. Xing and T. S. Rappaport, "Propagation measurement system and approach at 140 GHz-moving to 6G and above 100 GHz," in *2018 IEEE Global Communications Conference (GLOBECOM)*, Dec. 2018, pp. 1–6.

[56] S. Ju and T. S. Rappaport, "Millimeter-wave extended NYUSIM channel model for spatial consistency," in *2018 IEEE Global Communications Conference (GLOBECOM)*, Dec. 2018, pp. 1–6.

Theodore S. Rappaport (S'83–M'84–SM'91–F'98) is the David Lee/Ernst Weber Professor at New York University (NYU) and holds faculty appointments in the Electrical and Computer Engineering department of the NYU Tan- don School of Engineering, the Courant Computer Science department, and the NYU Langone School of Medicine. He is the founder and director of NYU WIRELESS, a multidisciplinary research center focused on the future of wireless communications and applications. His research has led the way for modern wireless communication systems. In 1987, his Ph.D. at Purdue University provided fundamental knowledge of indoor wireless channels used to create the first Wi-Fi standard (IEEE 802.11), and he conducted fundamental work that led to the first US Digital cellphone standards, TDMA IS-54/IS-136 and CDMA IS-95. He and his students engineered the worlds first public wi-fi hotspots, and more recently, his work proved the viability of millimeter waves for mobile communications. The global wireless industry adopted his vision for 5th generation (5G) cellphone networks. He founded three academic wireless research centers at Virginia Tech, University of Texas, and NYU that have produced thousands of engineers and educators since 1990, and has co-authored over 300 papers and twenty books, including the most cited books on wireless communications, adaptive antennas, wireless simulation, and millimeter-wave communications. He co- founded two wireless companies, TSR Technologies and Wireless Valley Communication, which were sold to publicly traded companies, and has advised many others. He co-founded the Virginia Tech Summer School and Wireless Symposium in 1991, the Texas Wireless Summit in 2003, and the Brooklyn 5G Summit (B5GS) in 2014. He has more than 100 patents, has served on the Technological Advisory Council of the Federal Communications Commission (FCC), is Fellow of the IEEE, Fellow of the Radio Club of America, Fellow of the National Academy of Inventors, a life member of the American Radio Relay League, a licensed professional engineer in Texas and Virginia, and an amateur radio operator (N9NB). He has received ASEEs Terman award, The Sir Monty Finniston Medal from the Institution of Engineering and Technology (IET), the IEEE Vehicular Technology Societys James R. Evans Avant Garde and Stu Meyer awards, the IEEE Education Society William E. Sayle award for achievement in education, the IEEE Communications Society Armstrong award, and the Armstrong Medal from the Radio Club of America..

George R. MacCartney, Jr. (S'08) received the B.S. and M.S. degrees in electrical engineering from Villanova University, Villanova, PA, USA, in 2010 and 2011, respectively. He received the Ph.D. degree in electrical engineering in 2018 with the NYU WIRELESS Research Center, New York University (NYU) Tandon School of Engineering, Brooklyn, NY, USA. He is a recipient of the 2016 Paul Baran Young Scholar Award from the Marconi Society. He also received the 2017 Dante Youla Award for Graduate Research Excellence in Electrical and Computer Engineering from the NYU Tandon School of Engineering ECE Department. He has authored or co-authored over 40 technical papers in the field of millimeter-wave (mmWave) propagation. His research interests include radio propagation, channel sounding, and channel modeling for ultra-wideband communications systems. He is currently a wireless systems engineer at Apple Inc.